Electroweak radiative corrections to $p^{(-)}p \to W^{\pm} \to \ell^{\pm}\nu$ beyond the pole approximation

U. Baur* and D. Wackeroth†

Department of Physics, State University of New York at Buffalo, Buffalo, New York 14260, USA

(Received 19 May 2004; published 28 October 2004)

We present a calculation of the complete electroweak $\mathcal{O}(\alpha)$ corrections to $p^{(-)}p \to W^{\pm} \to \ell^{\pm}\nu X$ ($\ell = e, \mu$) in the standard model of electroweak interactions, focusing on those corrections which do not contribute in the pole approximation. We study in detail the effect of these corrections on the transverse mass distribution, the W-width measurement, and the transverse mass ratio and cross section ratio of W and Z bosons.

DOI: 10.1103/PhysRevD.70.073015 PACS numbers: 12.15.Lk

I. INTRODUCTION

The standard model (SM) of electroweak interactions so far withstood all experimental challenges and is tested as a quantum field theory at the 0.1% level [1]. However, the mechanism of mass generation in the SM predicts the existence of a Higgs boson which, so far, has eluded direct observation. Direct searches at LEP2 give a 95% confidence-level lower bound on the mass of the SM Higgs boson of $M_H > 114.4$ GeV [2]. Indirect information on the mass of the Higgs boson can be extracted from the M_H dependence of radiative corrections to the W boson mass. With the present knowledge of the W boson and top quark masses [1,3], and the electromagnetic coupling constant, $\alpha(M_Z^2)$ [4], the SM Higgs boson mass can be indirectly constrained to $M_H = 113^{+62}_{-42}$ GeV [1,5] by a global fit to all electroweak precision data. Future more precise measurements of the W boson and top quark masses are expected to considerably improve the present indirect bound on M_H: with a precision of 27 MeV for the W boson mass, M_W, and 2.7 GeV for the top quark mass, which are target values for the expected integrated luminosity of 2 fb^{-1} of Run II of the Tevatron, M_H can be predicted with an uncertainty of about 35% [6]. In addition, the confrontation of a precisely measured W boson mass with the indirect SM prediction from a global fit to all electroweak precision data, $M_W = 80.386 \pm 0.023$ GeV [1], will provide a stringent test of the SM. A precise measurement of the W width, Γ_W, and comparison with the SM prediction, will help to further scrutinize the SM. The W width is expected to be measured in Run II with a precision of about 25–30 MeV from the high transverse mass tail when data from both lepton channels and both experiments are combined [7]. It can also be determined indirectly from the cross section ratio [8,9],

$$R_{W/Z} = \frac{\sigma(p\bar{p} \to W \to \ell\nu X)}{\sigma(p\bar{p} \to Z \to \ell^+\ell^- X)}, \tag{1}$$

together with the theoretical prediction for the ratio of the total W and Z production cross sections, the LEP measurement of the branching ratio $B(Z \to \ell^+\ell^-)$ [1], and the SM prediction for the $W \to \ell\nu$ decay width.

In hadronic collisions, the W mass is usually determined from the transverse mass distribution of the lepton and neutrino which originate from the W decay, $W \to \ell\nu$. The experimental uncertainty on M_W strongly depends on an accurate measurement of the transverse momentum of the neutrino which requires that the transverse momentum distribution of the W is well understood. In lowest order, the W is produced without any transverse momentum. Only when QCD corrections are taken into account does the W acquire a nonzero transverse momentum, p_T^W. For a detailed understanding of the p_T^W distribution, it is necessary to resum the soft gluon emission terms [10], and to model nonperturbative QCD corrections [11]. In addition to QCD corrections, electroweak (EW) radiative corrections play an important role in the W mass and width measurement; final state photon radiation is known to shift both quantities by $\mathcal{O}(100$ MeV) [12–17]. In order to measure the W mass and width with high precision at a hadron collider, it is thus necessary to fully understand and control higher order QCD and electroweak corrections. In the last few years, significant progress in our understanding of the EW corrections to W boson production in hadronic collisions has been made. A calculation of the $\mathcal{O}(\alpha)$ EW corrections to $p^{(-)}p \to W^{\pm} \to \ell^{\pm}\nu$ ($\ell = e, \mu$) in the pole approximation (PA) was presented in Ref. [18]. The complete $\mathcal{O}(\alpha)$ corrections were calculated in Ref. [19]. Two photon radiation in W production and decay has been calculated in Ref. [20]. Finally, first steps towards going beyond fixed order in EW radiative corrections were taken in Refs. [21,22] by including the effects of final state multiphoton radiation in W production, and in Ref. [23] where final state photon radiation was added to a calculation of W boson production which includes resummed QCD corrections.

In this paper we present an independent calculation of the complete $\mathcal{O}(\alpha)$ EW radiative corrections to $p^{(-)}p \to W^{\pm} \to \ell^{\pm}\nu$ using the methods developed in Ref. [24],

*email: baur@ubhex.physics.buffalo.edu
†email: dow@ubpheno.physics.buffalo.edu

 © 2004 The American Physical Society

and examine how the nonresonant corrections neglected in Ref. [18] affect several observables of interest, in particular, the measurement of the width of the W boson. Preliminary results of our calculation were reported in Ref. [25]. For the numerical evaluation, we use the Monte Carlo phase space slicing method for next-to-leading-order (NLO) calculations described in Ref. [26]. With the Monte Carlo method, it is easy to calculate a variety of observables simultaneously and to simulate detector response. The collinear singularities associated with initial state photon radiation are removed by universal collinear counter terms generated by "renormalizing" the parton distribution functions (PDFs) [18,27–30], in complete analogy to gluon emission in QCD. Final state charged lepton mass effects are included in our calculation in the following approximation. The lepton mass regularizes the collinear singularity associated with final state photon radiation. The associated mass singular logarithms of the form $\ln(\hat{s}/m_\ell^2)$, where $\hat{s}$ is the squared parton center-of-mass energy and m_ℓ is the charged lepton mass, are included in our calculation, but the very small terms of $\mathcal{O}(m_\ell^2/\hat{s})$ are neglected.

The technical details of our calculation are described in Sec. II. The electroweak $\mathcal{O}(\alpha)$ corrections consist of the electroweak one-loop contributions, including virtual photons, and of the emission of a real photon. To regularize the ultraviolet divergences associated with the virtual corrections, we use dimensional regularization in the ON SHELL renormalization scheme [31]. The nonresonant corrections are small in the W pole region, but become important at high $\ell\nu$ invariant masses, $m(\ell\nu)$, due to the presence of large Sudakov-like electroweak logarithms of the form $(\alpha/\pi)\ln^2[m(\ell\nu)/M_V]$ $(V = W, Z)$ [32].

Numerical results for the Tevatron ($p\bar{p}$ collisions at $\sqrt{s} = 2$ TeV) and the CERN Large Hadron collider (LHC, pp collisions at $\sqrt{s} = 14$ TeV) are presented in Sec. III. For $\ell\nu$ transverse masses above the W peak region, the nonresonant corrections reduce the differential cross section by $\mathcal{O}(10\%)$. We study in detail how these corrections affect the measurement of the W width from the tail of the transverse mass distribution. Using the results of Ref. [33], we also consider how the ratio of the W and Z cross sections, $R_{W/Z}$ (see Eq. (1)), and the transverse mass ratio of W and Z bosons are influenced. Finally, our conclusions are presented in Sec. IV.

II. THE $\mathcal{O}(\alpha)$ ELECTROWEAK RADIATIVE CORRECTIONS TO W PRODUCTION: RESONANT AND NONRESONANT CONTRIBUTIONS

The complete $\mathcal{O}(\alpha^3)$ parton-level cross section of W production via the Drell-Yan mechanism $q_i\bar{q}_{i'} \to f\bar{f}'(\gamma)$ is given by

$$d\hat{\sigma}^{(0+1)}(\hat{s},\hat{t}) = d\hat{\sigma}^{(0)} + d\hat{\sigma}_{\rm virt} + \sum_{a=\text{initial,final,}\atop\text{interf.}} [d\hat{\sigma}^{(0)} F^a_{BR} + d\hat{\sigma}^a_{2\to 3}], \quad (2)$$

where the Born cross section, $d\hat{\sigma}^{(0)}$, is of Breit-Wigner form and $\hat{s}$ and $\hat{t}$ are the usual Mandelstam variables in the parton center-of-mass frame. The corresponding Feynman diagrams are shown in Fig. 1 and 2. $d\hat{\sigma}_{\rm virt}$ describes the complete set of virtual $\mathcal{O}(\alpha)$ contributions consisting of the pure weak and the photonic virtual corrections:

$$d\hat{\sigma}_{\rm virt}(\hat{s},\hat{t}) = d\hat{\sigma}^{(0)} 2\mathcal{R}e[F_{\rm weak}(\hat{s}) + F_\gamma(\hat{s},\hat{t})] + d\hat{\sigma}_{WZ\rm box}(\hat{s},\hat{t}). \quad (3)$$

Explicit expressions for the pure weak form factor $F_{\rm weak}$ and for the contribution of the W, Z box diagrams, $d\hat{\sigma}_{WZ\rm box}$, are given in Appendix A. The form factors F^a_{BR} of Eq. (2) describing the initial state, final state and interference contribution of real soft photon radiation, and the photonic form factor F_γ can be found in Ref. [24] (Appendix D).

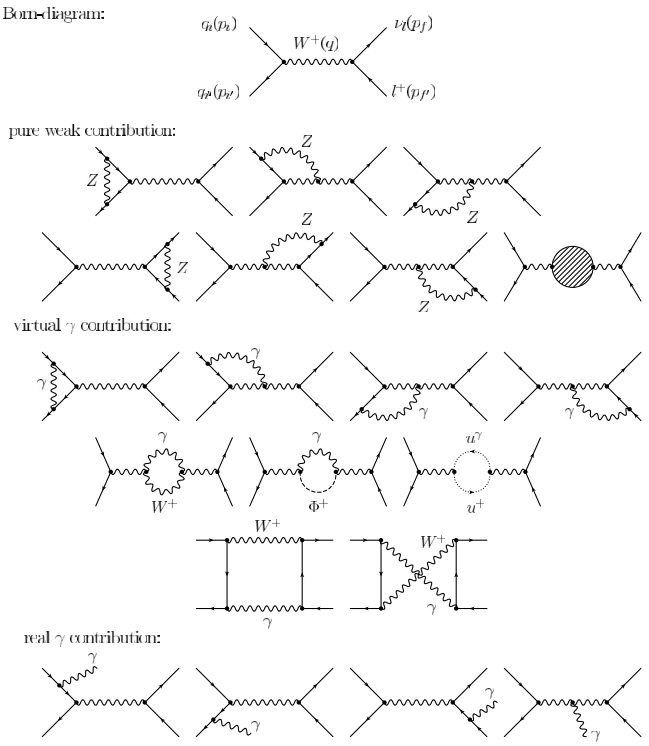

FIG. 1. The Feynman diagrams contributing to W boson production at $\mathcal{O}(\alpha^3)$ in the Feynman-'t Hooft gauge (Φ^+: Higgs-ghost field, u^+, u^γ: Faddeev-Popov-ghost fields; the nonphotonic contribution to the W self-energy insertion is symbolized by the shaded loop). An explicit representation of the nonphotonic contribution to the W self-energy insertion can be found in Ref. [64].

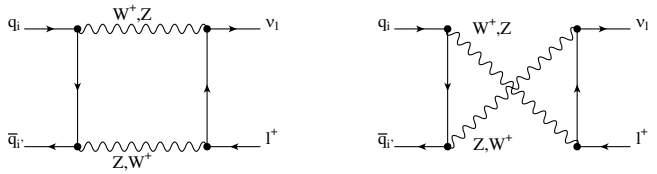

FIG. 2. Feynman diagrams for the W, Z box diagrams.

The soft photon region is defined by requiring that the photon energy in the parton center-of-mass frame, $\hat{E}_\gamma$, is smaller than a cutoff $\Delta E = \delta_s\sqrt{\hat{s}}/2$. In this phase space region, the soft photon approximation can be used to calculate the cross section as long as δ_s is sufficiently small. Throughout the calculation the soft singularities have been regularized by giving the photon a fictitious mass. As usual, the unphysical photon mass dependence cancels in the sum of the virtual and soft photon terms, $2\mathcal{R}eF_\gamma + \sum_a F^a_{BR}$. The IR finite contribution $d\hat{\sigma}^a_{2\to3}$ describes real photon radiation with $\hat{E}_\gamma > \Delta E$. The superscript a denotes the initial state, final state or interference contributions. Throughout the calculation of the $\mathcal{O}(\alpha)$ corrections we consider the fermions as being massless. We retain finite fermion masses only to regularize the collinear singularities which arise when the photon is emitted collinearly with one of the charged fermions. Thus, $d\hat{\sigma}^a_{2\to3}$ and the form factors F^a_{BR} and F_γ contain large mass singular logarithms which have to be treated with special care. For final state photon radiation, the collinear singularity is regularized by the finite lepton mass. In sufficiently inclusive measurements, the mass singular logarithmic terms originating from the collinear singularity cancel [34]. For initial state photonic corrections, however, the mass singular logarithms always survive. These singularities are universal to all orders in perturbation theory and can be absorbed by a redefinition (*renormalization*) of the PDFs [18,27]. This can be done in complete analogy to the calculation of QCD radiative corrections. As a result, the renormalized parton distribution functions become dependent on the QED factorization scale $\mu_{\rm QED}$ which is controlled by the well-known Gribov-Lipatov-Altarelli-Parisi (GLAP) equations [35]. These universal photonic corrections can be taken into account by a straightforward modification [28–30] of the standard GLAP evolution equations.

The QED induced terms in the GLAP equations lead to small corrections at the permille level to the distribution functions for most values of x and $\mu^2_{\rm QED}$ [30,36]. Only at large $x \gtrsim 0.5$ and large $\mu^2_{\rm QED} \gtrsim 10^3$ GeV^2 do the corrections reach the magnitude of one percent.

In order to treat the $\mathcal{O}(\alpha)$ initial state photonic corrections to W production in hadronic collisions in a consistent way, QED corrections should be incorporated in the global fitting of the PDFs, i.e., all data which are used to fit the parton distribution functions should be corrected for QED effects. Current fits [37,38] to the PDFs do not include QED corrections. The missing QED corrections introduce an uncertainty which, however, is probably much smaller than the present experimental uncertainties on the parton distribution functions.

Absorbing the collinear singularity into the PDFs introduces a QED factorization scheme dependence. The squared matrix elements for different QED factorization schemes differ by the finite $\mathcal{O}(\alpha)$ terms which are absorbed into the PDFs in addition to the singular terms. Our calculation has been carried out both in the QED $\overline{\rm MS}$ and DIS schemes, which are defined analogously to the usual $\overline{\rm MS}$ [39] and DIS [40] schemes used in QCD calculations. All numerical calculations in this paper are performed using the QED DIS scheme. The QED DIS scheme is defined by requiring the same expression for the leading and next-to-leading-order structure function F_2 in deep inelastic scattering, which is given by the sum of the quark distributions. Since F_2 data are an important ingredient in extracting PDFs, the effect of the $\mathcal{O}(\alpha)$ QED corrections on the PDFs should be reduced in the QED DIS scheme.

In the vicinity of the W resonance, the W, Z box diagrams of Fig. 2 can be neglected as nonresonant contributions of higher order in perturbation theory, and, as demonstrated in [24], a gauge invariant decomposition of the complete $\mathcal{O}(\alpha)$ contribution into a QED-like and a modified weak part can be performed. Unlike the Z boson case, the Feynman diagrams of Fig. 1 which involve a virtual photon do not represent a gauge invariant subset. In Ref. [24], it was demonstrated that gauge invariant contributions can be extracted from the infrared singular virtual photonic corrections, $\tilde{F}^a_{\rm YFS}$ (the modified Yennie-Frautschi-Suura, YFS, form factors). These contributions can be combined with the real photon corrections in the soft photon region, F^a_{BR}, to form gauge invariant QED-like contributions corresponding to initial state, final state and interference corrections. The IR finite remainder of the virtual photonic corrections and the pure weak one-loop corrections of Fig. 1 can be combined to separately gauge invariant modified weak contributions to the W boson production and decay processes.

Both the QED-like and the modified weak contributions can be expressed in terms of form factors, $F^a_{\rm QED}$ and $\tilde{F}^a_{\rm weak}$, which multiply the Born cross section [24]. Thus, the complete $\mathcal{O}(\alpha^3)$ parton-level cross section of resonant W production via the Drell-Yan mechanism $q_i\overline{q}_{i'} \to ff'(\gamma)$ can be expressed in the form

$$d\hat{\sigma}^{(0+1)}_{\rm res} = d\hat{\sigma}^{(0)}[1 + 2\mathcal{R}e(\tilde{F}^{\rm initial}_{\rm weak} + \tilde{F}^{\rm final}_{\rm weak})(M^2_W)] + \sum_{\substack{a={\rm initial,final,}\\ {\rm interf.}}} [d\hat{\sigma}^{(0)}F^a_{\rm QED}(\hat{s},\hat{t}) + d\hat{\sigma}^a_{2\to3}]. \quad (4)$$

The modified weak contributions have to be evaluated at

$\hat{s} = M_W^2$. Explicit expressions for the form factors $F^a_{\rm QED}$, $\tilde{F}^a_{\rm weak}$ are given in Ref. [24].

The nonresonant part, which was neglected in Refs. [18,24], can then be obtained from the resonant contribution, $d\hat{\sigma}^{(0+1)}_{\rm res}$ (see Eq. (4)), and the complete $\mathcal{O}(\alpha)$ contribution, $d\hat{\sigma}^{(0+1)}$ of Eq. (2):

$$\begin{aligned} d\hat{\sigma}_{\rm nonres}(\hat{s},\hat{t}) &= d\hat{\sigma}^{(0+1)} - d\hat{\sigma}^{(0+1)}_{\rm res} \\ &= d\hat{\sigma}_{WZ\rm box}(\hat{s},\hat{t}) + d\hat{\sigma}^{(0)} \\ &\quad \times 2\mathcal{R}e\Bigg\{\sum_{a=\text{initial,final}} [F^a_{\rm weak}(\hat{s}) - \tilde{F}^a_{\rm weak}(M_W^2)] \\ &\quad + \Bigg(F_\gamma - \sum_{\substack{a=\text{initial,final,}\\ \text{interf.}}} \tilde{F}^a_{\rm YFS}\Bigg)(\hat{s},\hat{t})\Bigg\}, \end{aligned} \tag{5}$$

where we have used Eq. (A1) and $F^a_{\rm QED} = F^a_{BR} + 2\mathcal{R}e\tilde{F}^a_{\rm YFS}$ (a = initial, final, interf.). Equation (5) shows that the nonresonant contribution consists of the W, Z box contributions, the IR finite remnants of the virtual photon one-loop corrections which are not included in the YFS form factor, and the $\hat{s}$-dependent parts of the pure weak vertex and self-energy one-loop corrections, which have been neglected when evaluating the pure weak form factor at $\hat{s} = M_W^2$. $d\hat{\sigma}_{\rm nonres}$ is free of mass singularities (terms proportional to $\ln(\hat{s}/m_f^2)$, where m_f is the mass of an initial state or final state fermion) and on-shell singularities, i.e., logarithms of the form $\ln(|\hat{s} - M_W^2|)$. It represents a gauge invariant subset of the complete $\mathcal{O}(\alpha)$ contribution to the W production process $q_i\bar{q}_{i'} \to f\bar{f}'$, and its numerical impact can thus be studied separately. In Fig. 3 we illustrate the effect of the nonresonant contribution on the total parton-level cross section by showing the variation of the relative correction $\delta = \hat{\sigma}_{\rm nonres}/\hat{\sigma}^{(0)}$ (in percent) with $\sqrt{\hat{s}}$ where $\hat{\sigma}^{(0)}$ is the Born cross section,

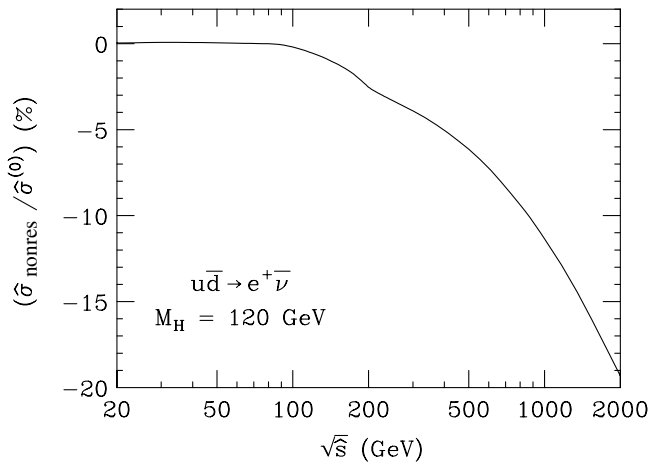

FIG. 3. The relative size (in percent) of the nonresonant $\mathcal{O}(\alpha)$ corrections to the Born $u\bar{d} \to W^+ \to \ell^+\nu$ parton-level total cross section as a function of the parton center-of-mass energy, $\sqrt{\hat{s}}$. The parameters used are listed in Eqs. (8)–(10).

$$\hat{\sigma}^{(0)} = \frac{\pi}{36}\alpha^2\left(1 - \frac{M_W^2}{M_Z^2}\right)^{-2} \frac{\hat{s}}{(\hat{s} - M_W^2)^2 + (\frac{\hat{s}}{M_W}\Gamma_W)^2}, \tag{6}$$

in the s-dependent width scheme [24]. As can be seen, the nonresonant contribution can be neglected in the vicinity of the W resonance but becomes increasingly important at large center-of-mass energies due to the occurrence of large, Sudakov-like logarithms of the form $(\alpha/\pi)\ln^2(\hat{s}/M_W^2)$. The kink at $\sqrt{\hat{s}} \approx 200$ GeV is due to the WH threshold in the W self-energy.

The observable $\mathcal{O}(\alpha^3)$ cross section is obtained by convoluting the parton cross section with the quark distribution functions $f_{q/A}(x, Q^2)$ ($\hat{s} = x_1x_2s$) and summing over all quark flavors q and q',

$$\begin{aligned} d\sigma(s) = \sum_{q,q'} \int_0^1 dx_1 dx_2 [&f_{q/A}(x_1, Q^2) f_{\bar{q}'/B}(x_2, Q^2) d\hat{\sigma}^{(0+1)} \\ &+ (q \leftrightarrow \bar{q}')] \end{aligned} \tag{7}$$

with $(A, B) = (p, \bar{p})$ for the Tevatron and (p, p) for the LHC. The parton distribution functions depend on the QCD renormalization and factorization scales, μ_r and μ_f, which we choose to be equal, $\mu_r = \mu_f = Q$.

III. PHENOMENOLOGICAL RESULTS

A. Preliminaries

We shall now discuss the phenomenological implications of the $\mathcal{O}(\alpha)$ nonresonant EW corrections to $\ell\nu$ production at the Tevatron ($p\bar{p}$ collisions at $\sqrt{s} =$ 2 TeV) and the LHC (pp collisions at $\sqrt{s} = 14$ TeV). For the numerical evaluation we chose the following set of SM input parameters [41]:

$$\begin{aligned} G_\mu &= 1.16639 \times 10^{-5}\ \text{GeV}^{-2}, \\ \alpha &= 1/137.035\,989\,5, & M_Z &= 91.1867\ \text{GeV}, \\ \alpha_s &\equiv \alpha_s(M_W^2) = 0.121, & m_e &= 0.510\,999\,07\ \text{MeV}, \\ m_\mu &= 0.105\,658\,389\ \text{GeV}, & m_\tau &= 1.777\ \text{GeV}, \\ m_u &= 0.0464\ \text{GeV}, & m_c &= 1.5\ \text{GeV}, \\ m_t &= 174\ \text{GeV}, & m_d &= 0.0465\ \text{GeV}, \\ m_s &= 0.15\ \text{GeV}, & m_b &= 4.7\ \text{GeV}, \\ |V_{ud}| &= |V_{cs}| = 0.97, & |V_{us}| &= |V_{dc}| = 0.22. \end{aligned} \tag{8}$$

The fermion masses only enter through loop contributions to the vector boson self-energies and as regulators of the collinear singularities which arise in the calculation of the QED contribution. Nonzero light quark masses are only used in the calculation of the vector boson self-energies. The light quark masses are chosen such that the value for the hadronic contribution to the photon vacuum polarization for five active flavors, $\Delta\alpha^{(5)}_{\rm had}(M_Z^2) = 0.028$ [4], which is derived from low-energy e^+e^- data with the help of dispersion relations, is recovered. V_{ij} are the matrix elements of the quark mixing matrix.

The W mass and the Higgs boson mass, M_H, are related via loop corrections. A parametrization of the W mass which, for 10 GeV $< M_H <$ 1 TeV, deviates by at most 0.5 MeV from the theoretical value including the full two-loop contributions is given in Ref. [42]. Here we use the somewhat older parametrization of Ref. [43],[1]

$$M_W = M_W^0 - 0.0581 \ln\left(\frac{M_H}{100\ \text{GeV}}\right) - 0.0078 \times \ln^2\left(\frac{M_H}{100\ \text{GeV}}\right) - 0.085\left(\frac{\alpha_s}{0.118} - 1\right) - 0.518 \times \left(\frac{\Delta\alpha^{(5)}_{\text{had}}(M_Z^2)}{0.028} - 1\right) + 0.537\left[\left(\frac{m_t}{175\ \text{GeV}}\right)^2 - 1\right] \tag{9}$$

with $M_W^0 = 80.3805$ GeV, which was used in the analysis of the LEP data. The parametrization of Eq. (9) reproduces the result of Ref. [43] to 0.2 MeV for 75 GeV $< M_H <$ 350 GeV. For the numerical discussion we choose

$$M_H = 120\ \text{GeV}, \tag{10}$$

which is consistent with current direct [2] and indirect bounds [1,5], and work in the s-dependent width scheme. For the input parameters listed in Eq. (8) we obtain $M_W = 80.3612$ GeV. Higher order (irreducible) corrections connected with the ρ-parameter are taken into account in our calculation by replacing

$$\frac{\delta M_Z^2}{M_Z^2} - \frac{\delta M_W^2}{M_W^2} \to \frac{\delta M_Z^2}{M_Z^2} - \frac{\delta M_W^2}{M_W^2} - \Delta\rho^{HO} \tag{11}$$

in the renormalized Z and γ, Z self-energies as described in Appendix B of Ref. [18]. The W width and the $q_i\bar{q}_{i'} \to f\bar{f}'(\gamma)$ amplitude are calculated in the G_μ scheme. In the G_μ scheme, the fine structure constant α is replaced with

$$\alpha \to \frac{\sqrt{2}G_\mu M_W^2}{\pi}\left(1 - \frac{M_W^2}{M_Z^2}\right), \tag{12}$$

and M_W is obtained from Eq. (9). For the W width, including $\mathcal{O}(\alpha)$ EW (see also Ref. [45]) and QCD corrections up to $\mathcal{O}(\alpha_s^3)$ [18,46,47], we obtain $\Gamma_W = 2.0721$ GeV.

In the numerical results presented below, we also take into account the leading $\mathcal{O}(\alpha^2)$ weak corrections to resonant W production which can be obtained by performing the following replacement in Eq. (4):

$$1 + 2\mathcal{R}e(\tilde{F}^{\text{initial}}_{\text{weak}} + \tilde{F}^{\text{final}}_{\text{weak}})(M_W^2) \to \left|\left[1 + \frac{1}{2}\tilde{F}^{\text{initial}}_{\text{weak}}(M_W^2)\right]\left[1 + \frac{1}{2}\tilde{F}^{\text{final}}_{\text{weak}}(M_W^2)\right]\right|^2. \tag{13}$$

The dominant nonphotonic electroweak corrections to resonant W production can be taken into account in the effective Born approximation (EBA) where the W cross section, σ^{EBA}, is calculated by replacing α in Eq. (6) with the expression given in Eq. (12) and using the W mass obtained from Eq. (9). In the following, we shall use the EBA cross section as a reference when discussing how the $\mathcal{O}(\alpha)$ EW corrections affect physical observables.

Following a brief comparison with the calculation of Ref. [19], we discuss the impact of the nonresonant EW corrections on the transverse mass distribution and how they affect the value of the W width extracted from that distribution. We then consider the W production cross section, the W to Z cross section ratio, and the W to Z transverse mass ratio. To compute the hadronic cross section we use the MRSR2 set of parton distribution functions [48], and take the renormalization scale μ_r and the QED and QCD factorization scales μ_{QED} and μ_{QCD} to be $\mu_r^2 = \mu_{\text{QED}}^2 = \mu_{\text{QCD}}^2 = M_W^2$. The detector acceptance is simulated by imposing the following transverse momentum (p_T) and pseudorapidity (η) cuts:

$$p_T(\ell) > 20\ \text{GeV}, \qquad |\eta(\ell)| < 2.5, \qquad \ell = e, \mu, \tag{14}$$

$$\not{p}_T > 20\ \text{GeV}, \tag{15}$$

where $\not{p}_T$ is the missing transverse momentum originating from the neutrino. These cuts approximately model the acceptance of the CDF II [49] and D0 [50] detectors at the Tevatron, and the ATLAS [51] and CMS [52] detectors at the LHC. Uncertainties in the energy measurements of the charged leptons in the detector are simulated in the calculation by Gaussian smearing of the particle four-momentum vector with standard deviation σ which depends on the particle type and the detector. The numerical results presented here were calculated using σ values based on the D0 and ATLAS specifications.

The granularity of the detectors and the size of the electromagnetic showers in the calorimeter make it difficult to discriminate between electrons and photons with a small opening angle. In such cases we recombine the four-momentum vectors of the electron and photon to an effective electron four-momentum vector. The exact recombination procedure is detector dependent. For calculations performed at Tevatron energies we use a procedure similar to that used by the D0 Collaboration in Run I, requiring that the electron and photon momentum four-vectors are combined into an effective electron momentum four-vector if their separation in the pseudo-rapidity-azimuthal angle plane,

$$\Delta R(e, \gamma) = \sqrt{[\Delta\eta(e, \gamma)]^2 + [\Delta\phi(e, \gamma)]^2}, \tag{16}$$

is $\Delta R(e, \gamma) < 0.2$. For $0.2 < \Delta R(e, \gamma) < 0.4$ events are rejected if $E_\gamma > 0.15E_e$. Here E_γ (E_e) is the energy of the photon (electron) in the laboratory frame. For events with $0.2 < \Delta R(e, \gamma) < 0.3$ and $E_\gamma < 0.15E_e$, the electron and photon momentum four-vectors are again

[1] An updated parametrization can be found in Ref. [44].

combined. At LHC energies, we recombine the electron and photon four-momentum vectors if $\Delta R(e,\gamma) < 0.07$, similar to the resolution expected for ATLAS [51]. Recombining the electron and photon four-momentum vectors eliminates the mass singular logarithmic terms originating from final state photon radiation and strongly reduces the size of the QED-like final state corrections [18].

Muons are identified by hits in the muon chambers and the requirement that the associated track is consistent with a minimum ionizing particle. This limits the photon energy for small muon-photon opening angles. For muons at the Tevatron, we again adopt the D0 specifications and require that the energy of the photon is $E_\gamma < 2$ GeV for $\Delta R(\mu,\gamma) < 0.2$, and $E_\gamma < 6$ GeV for $0.2 < \Delta R(\mu,\gamma) < 0.6$. At the LHC, following Ref. [51], we require the photon energy to be smaller than $E_c^\gamma = 5$ GeV if $\Delta R(\mu,\gamma) < 0.3$. The cut on the photon energy increases the size of the photonic corrections for $m(\mu\nu) > 100$ GeV [18]. For future reference, we summarize the lepton identification requirements in Table I.

We use the input parameters listed in Eq. (8) and impose the cuts and lepton identification requirements described above in all subsequent numerical simulations, unless explicitly noted otherwise.

B. Comparison with Ref. [19]

As mentioned before, the matrix elements of the full $\mathcal{O}(\alpha)$ EW corrections to $q\bar{q}' \to \ell\nu + X$ were presented in Ref. [19], together with a discussion of how EW radiative corrections influence the p_T distribution of the charged lepton, and the transverse mass distribution. In this section we compare the integrated cross sections given in Ref. [19] for different ranges in $p_T(\ell)$ at the Tevatron and LHC with the results of our calculation, using the input parameters, PDFs, cuts, and the lepton-photon recombination procedure of Ref. [19]. The results are shown in Table II. The table lists the lowest order cross section in the G_μ scheme, $\sigma^{(0)}$, and the relative corrections,

$$\delta = \frac{\sigma^{\mathcal{O}(\alpha^3)} - \sigma^{(0)}}{\sigma^{(0)}} \tag{17}$$

for the full $\mathcal{O}(\alpha)$ EW corrections, and

$$\delta_{PA} = \frac{\sigma^{PA} - \sigma^{(0)}}{\sigma^{(0)}} \tag{18}$$

for the $\mathcal{O}(\alpha)$ EW corrections in the pole approximation. Our results are found to agree within the statistical accuracy of the Monte Carlo integration with those obtained in Ref. [19] over the entire lepton p_T range with exception of the region $p_T(\ell) \geq 500$ GeV at the LHC where a slight discrepancy in δ is observed. The discrepancy could be due to a different numerical implementation of the box diagrams here and in Ref. [19].

C. Nonresonant Corrections to the Transverse Mass Distribution

Table II shows that the nonresonant EW corrections quickly become important for transverse momenta above the Jacobian peak region, $p_T(\ell) > M_W/2 \approx 40$ GeV. The deviation of the $\mathcal{O}(\alpha^3)$ cross section in the pole approximation from the full NLO result at large $p_T(\ell)$ is due to large Sudakov-like electroweak logarithms of the form $(\alpha/\pi)\ln^2[m(\ell\nu)/M_V]$ $(V = W, Z)$ [32] which mostly arise from the contribution of the W, Z box diagrams and to a lesser extent from the energy dependence of the form factors F^a_{weak} and $F_\gamma - \sum_a \tilde{F}^a_{\text{YFS}}$. The same qualitative behavior is also expected for the transverse mass distribution, which is used to determine the W mass and width [14]. The transverse mass is defined by

$$M_T = \sqrt{2p_T(\ell)p_T(\nu)(1 - \cos\phi^{\ell\nu})}, \tag{19}$$

where $p_T(\nu)$ is the transverse momentum of the neutrino, and $\phi^{\ell\nu}$ is the angle between the charged lepton and the neutrino in the transverse plane. The neutrino transverse momentum is identified with the missing transverse momentum, $\not{p}_T$, in the event.

The ratio of the complete $\mathcal{O}(\alpha^3)$ electroweak and the EBA differential cross section as a function of M_T is

TABLE I. Summary of lepton identification requirements.

Tevatron	
Electrons	Muons
Combine e and γ momentum four-vectors if $\Delta R(e,\gamma) < 0.2$ and if $E_\gamma < 0.15E_e$ for $0.2 < \Delta R(e,\gamma) < 0.3$ Reject events with $E_\gamma > 0.15E_e$ for $0.2 < \Delta R(e,\gamma) < 0.4$	Reject events with $E_\gamma > 2$ GeV for $\Delta R(\mu,\gamma) < 0.2$ Reject events with $E_\gamma > 6$ GeV for $0.2 < \Delta R(\mu,\gamma) < 0.6$
LHC	
Electrons	Muons
Combine e and γ momentum four-vectors if $\Delta R(e,\gamma) < 0.07$	Reject events with $E_\gamma > 5$ GeV for $\Delta R(\mu,\gamma) < 0.3$

TABLE II. Integrated lowest order cross sections in the G_μ scheme, $\sigma^{(0)}$, the relative corrections for the pole approximation ,$\delta_{\rm PA}$, and the full $\mathcal{O}(\alpha)$ EW corrections, δ, for several ranges of $p_T(\ell)$. Shown are the results of our calculation and of Ref. [19] for (a) $p\bar{p} \to \ell\nu$ at $\sqrt{s} = 2$ TeV and (b) $pp \to \ell\nu$ at $\sqrt{s} = 14$ TeV. The statistical uncertainties of the Monte Carlo integration are also shown. The lepton and photon momenta are recombined for small values of $\Delta R(\ell, \gamma)$ using the simplified procedure described in Ref. [19]. We also use the same input parameters, PDFs, and cuts as Ref. [19].

(a) $p\bar{p} \to \ell\nu$, $\sqrt{s} = 2$ TeV

$p_T(\ell)$ (GeV)	$25 - \infty$	$50 - \infty$	$75 - \infty$	$100 - \infty$	$200 - \infty$	$300 - \infty$
$\sigma^{(0)}$ (pb) Ref. [19]	407.03(5)	2.481(1)	0.3991(1)	0.1305(1)	0.006020(2)	0.0004821(1)
$\sigma^{(0)}$ (pb) this calc.	407.02(7)	2.4817(6)	0.39926(9)	0.13058(3)	0.006017(2)	0.0004821(3)
δ (%) Ref. [19]	−1.8(1)	−2.7(1)	−4.8(1)	− 6.3(1)	− 10.4(1)	− 13.6(1)
δ (%) this calc.	−1.7(1)	−2.5(1)	−4.7(1)	− 6.1(1)	− 10.1(1)	− 13.3(1)
$\delta_{\rm PA}$ (%) Ref. [19]	−1.7(1)	−1.6(1)	−2.3(1)	− 2.5(1)	− 3.3(1)	− 3.9(1)
$\delta_{\rm PA}$ (%) this calc.	−1.7(1)	−1.5(1)	−2.2(1)	− 2.4(1)	− 3.1(1)	− 3.7(1)

(b) $pp \to \ell\nu$, $\sqrt{s} = 14$ TeV

$p_T(\ell)$ (GeV)	$25 - \infty$	$50 - \infty$	$100 - \infty$	$200 - \infty$	$500 - \infty$	$1000 - \infty$
$\sigma^{(0)}$ (pb) Ref. [19]	1933.5(3)	11.50(1)	0.8198(4)	0.1015(1)	0.005277(1)	0.0003019(1)
$\sigma^{(0)}$ (pb) this calc.	1933.4(3)	11.499(2)	0.8202(1)	0.10155(2)	0.005277(1)	0.0003019(1)
δ (%) Ref. [19]	−1.8(1)	−2.7(1)	−6.2(1)	− 10.2(1)	− 19.6(1)	− 29.6(1)
δ (%) this calc.	−1.8(1)	−2.3(1)	−6.0(1)	− 10.1(1)	− 19.1(1)	− 28.6(1)
$\delta_{\rm PA}$ (%) Ref. [19]	−1.8(1)	−1.5(1)	−1.6(1)	− 1.6(1)	− 2.4(1)	− 3.6(1)
$\delta_{\rm PA}$ (%) this calc.	−1.8(1)	−1.2(1)	−1.5(1)	− 1.6(1)	− 2.4(1)	− 3.4(1)

shown in Fig. 4. In order to make the effect of the nonresonant weak corrections more transparent, we also show the corresponding ratio for the case of the $\mathcal{O}(\alpha)$ EW corrections in the pole approximation (dashed lines) [18]. For $M_T \leq M_W$, the pole approximation is seen to very well represent the complete electroweak $\mathcal{O}(\alpha)$ corrections. In this region, the shape change in the M_T distribution is largely due to the contribution of the final state QED-like corrections. Because of the recombination of electrons and photons, the EW corrections in the pole approximation reduce the $e\nu(\gamma)$ differential cross section by only 2%–3% over the transverse mass region considered. In the muon case, the cut on the photon energy for photons which have a small opening angle with the muon reduces the hard photon part of the $\mathcal{O}(\alpha^3)$ $\mu\nu(\gamma)$ cross section. As a result, the QED-like corrections are much more pronounced and display a much stronger dependence on the transverse mass than in the electron case. Without taking the lepton identification criteria of Table I into account, the QED-like corrections in the electron case are larger, due to the mass singular logarithmic corrections which originate from final state photon radiation. The nonresonant EW corrections are seen to increase rapidly in size with M_T. For $M_T = 300$ GeV, they reduce the cross section by about 4% at the Tevatron. The dotted lines, finally, show the cross section ratio when the $p\bar{p} \to W^+(\to \ell^+\nu)Z(\to \bar{\nu}\nu)$ background is included in addition to the complete $\mathcal{O}(\alpha)$ EW corrections. The WZ background is seen to be much smaller than the $\mathcal{O}(\alpha)$ EW corrections.

Figure 5 shows the corresponding results for the LHC in the high transverse mass tail. For $M_T > 1.5$ TeV, the nonresonant $\mathcal{O}(\alpha)$ EW corrections reduce the differential cross section by 20% or more and thus are of the same size as the $\mathcal{O}(\alpha_s)$ corrections. This is larger than the expected statistical uncertainty in a 200 GeV bin centered at $M_T = 1.5$ TeV for 100 fb^{-1}. It will thus be important to take into account the nonresonant weak corrections when searching for new heavy W bosons, such as Kaluza-Klein excitations of the W appearing in TeV-scale models with extra dimensions [53], at the LHC. The results shown in Fig. 5, however, should be interpreted with caution. Since the nonresonant weak corrections become large for transverse masses above one TeV, they need to be resummed in order to obtain accurate predictions in this phase space region (for a recent review of the resummation of electroweak Sudakov-like logarithms see Ref. [54]). Although the resummation of electroweak Sudakov-like logarithms in general four fermion electroweak processes has been discussed in the literature [32,55], a calculation of $\ell\nu$ production in hadronic collisions which includes resummation of electroweak logarithms has not been carried out yet.

D. Nonresonant EW Radiative Corrections and the W Width

We now discuss how the nonresonant $\mathcal{O}(\alpha)$ EW corrections affect the W width determined from the high transverse mass tail. In Run I of the Tevatron, Γ_W has been measured by the CDF and D0 Collaborations using this technique with a combined uncertainty of 105 MeV [14]. In Run II, with an integrated luminosity of 2 fb^{-1}, one expects to achieve a precision of 50 MeV per lepton

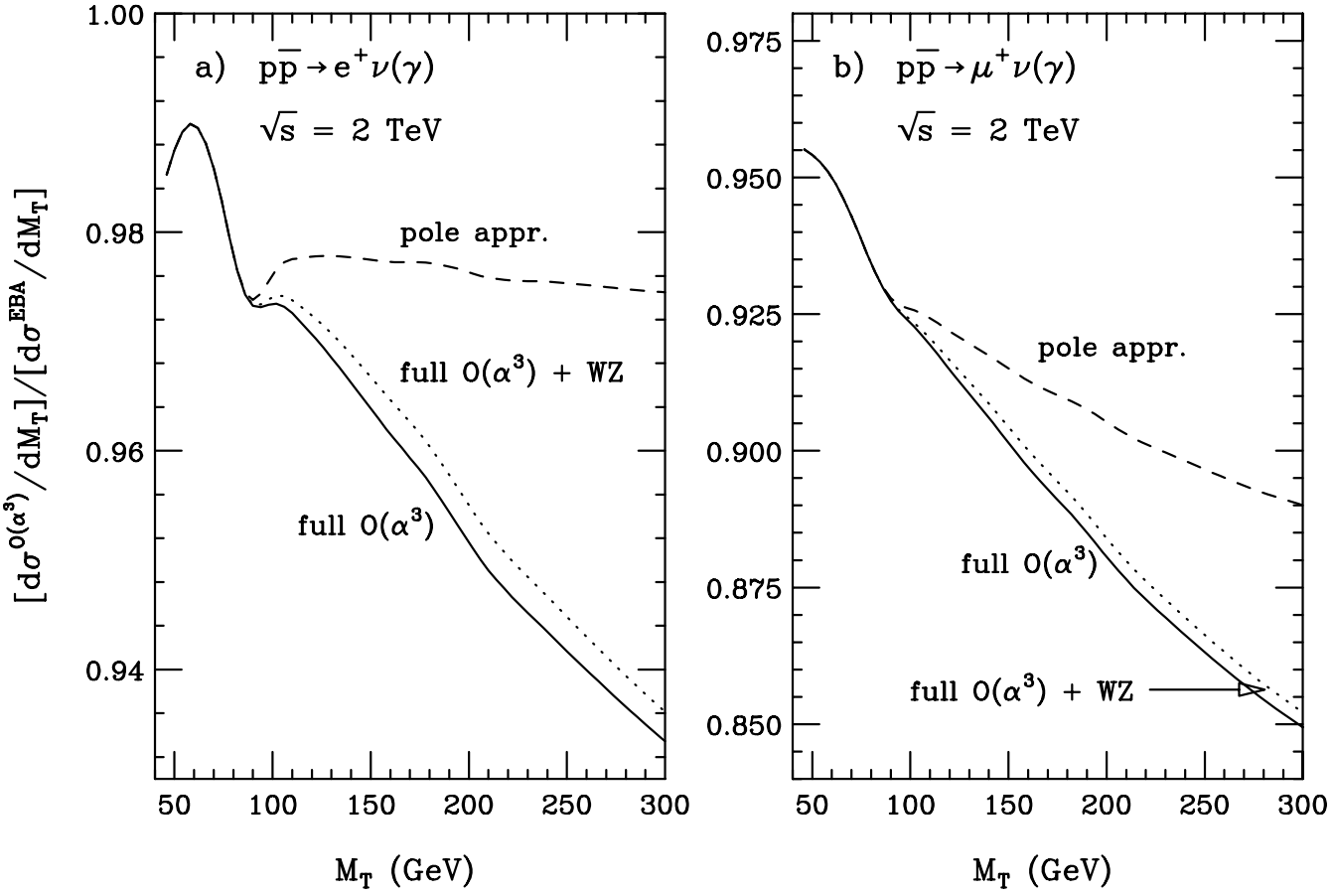

FIG. 4. The ratio $[d\sigma^{\mathcal{O}(\alpha^3)}/dM_T]/[d\sigma^{\mathrm{EBA}}/dM_T]$ as a function of the transverse mass for (a) $p\bar{p} \to e^+\nu_e(\gamma)$ and (b) $p\bar{p} \to \mu^+\nu_\mu(\gamma)$ at $\sqrt{s} = 2$ TeV. The solid lines show the ratio of the complete $\mathcal{O}(\alpha^3)$ electroweak and the EBA differential cross section. The dashed lines display the corresponding ratio for the case where only the resonant $\mathcal{O}(\alpha)$ EW corrections (see Eq. (4)) are taken into account (pole approximation). The dotted lines show the ratio when the $p\bar{p} \to W^+(\to \ell\nu)Z(\to \bar{\nu}\nu)$ background is included in addition to the complete $\mathcal{O}(\alpha)$ EW corrections. The cuts and lepton identification requirements imposed are described in Sec. III A.

channel and experiment [7]. Assuming that the error correlation of CDF and D0 data, as in Run I, is small [14] for the W-width measurement, this results in an expected overall uncertainty of $\delta\Gamma_W = 25 - 30$ MeV. In the experimental analysis, the measured transverse mass distribution is compared with the theoretical prediction for various values of the W width where the total cross section has been normalized to the experimental value [16,17]. This is equivalent to analyzing the normalized M_T distribution,

$$\frac{d\tilde{\sigma}}{dM_T}(\Gamma_W) = \frac{1}{\sigma_{\mathrm{tot}}(\Gamma_W)}\frac{d\sigma}{dM_T}(\Gamma_W), \tag{20}$$

where σ_{tot} is the total $\ell\nu(\gamma)$ cross section within cuts. At lowest order, the W width enters the cross section in the form of the squared W propagator (see Eq. (6)),

$$|D_W(\hat{s})|^2 = [(\hat{s} - M_W^2)^2 + \hat{s}^2\Gamma_W^2/M_W^2]^{-1}. \tag{21}$$

The lowest order total $\ell\nu$ production cross section thus is proportional to $1/\Gamma_W$. As a result, $d\tilde{\sigma}/dM_T$ is proportional to Γ_W for $M_T \gg M_W$. This is clearly displayed in the ratio of the normalized M_T distribution for arbitrary Γ_W to the normalized M_T distribution in the SM,

$$\mathcal{R}(\Gamma_W) = \frac{\frac{d\tilde{\sigma}}{dM_T}(\Gamma_W)}{\frac{d\tilde{\sigma}}{dM_T}(\Gamma_W^{SM})}, \tag{22}$$

where $\Gamma_W^{\mathrm{SM}} = 2.072$ GeV is the SM W width (see Sec. III A). $\mathcal{R}(\Gamma_W)$ in the pole approximation $\mathcal{R}_{\mathrm{PA}}(\Gamma_W)$ is shown in Fig. 6 for $p\bar{p} \to e^+\nu(\gamma)$ at the Tevatron with $\Gamma_W = \Gamma_W^{\mathrm{SM}} - 10$ MeV $= 2.062$ GeV (dotted line) and $\Gamma_W = \Gamma_W^{\mathrm{SM}} - 30$ MeV $= 2.042$ GeV (dashed line). Qualitatively similar results are obtained for the muon final state and at LHC energies. $\mathcal{R}_{\mathrm{PA}}(\Gamma_W)$ is seen to be almost constant and approximately equal to $\Gamma_W/\Gamma_W^{\mathrm{SM}}$ for $M_T > 100$ GeV. For $M_T < M_W$, the ratio is almost independent of Γ_W, and very close to one. If no detector resolution effects are taken into account, $d\tilde{\sigma}/dM_T$ is proportional to $1/\Gamma_W$ for $M_T = M_W$ at lowest order, resulting in an enhancement proportional to $\Gamma_W^{\mathrm{SM}}/\Gamma_W$ in

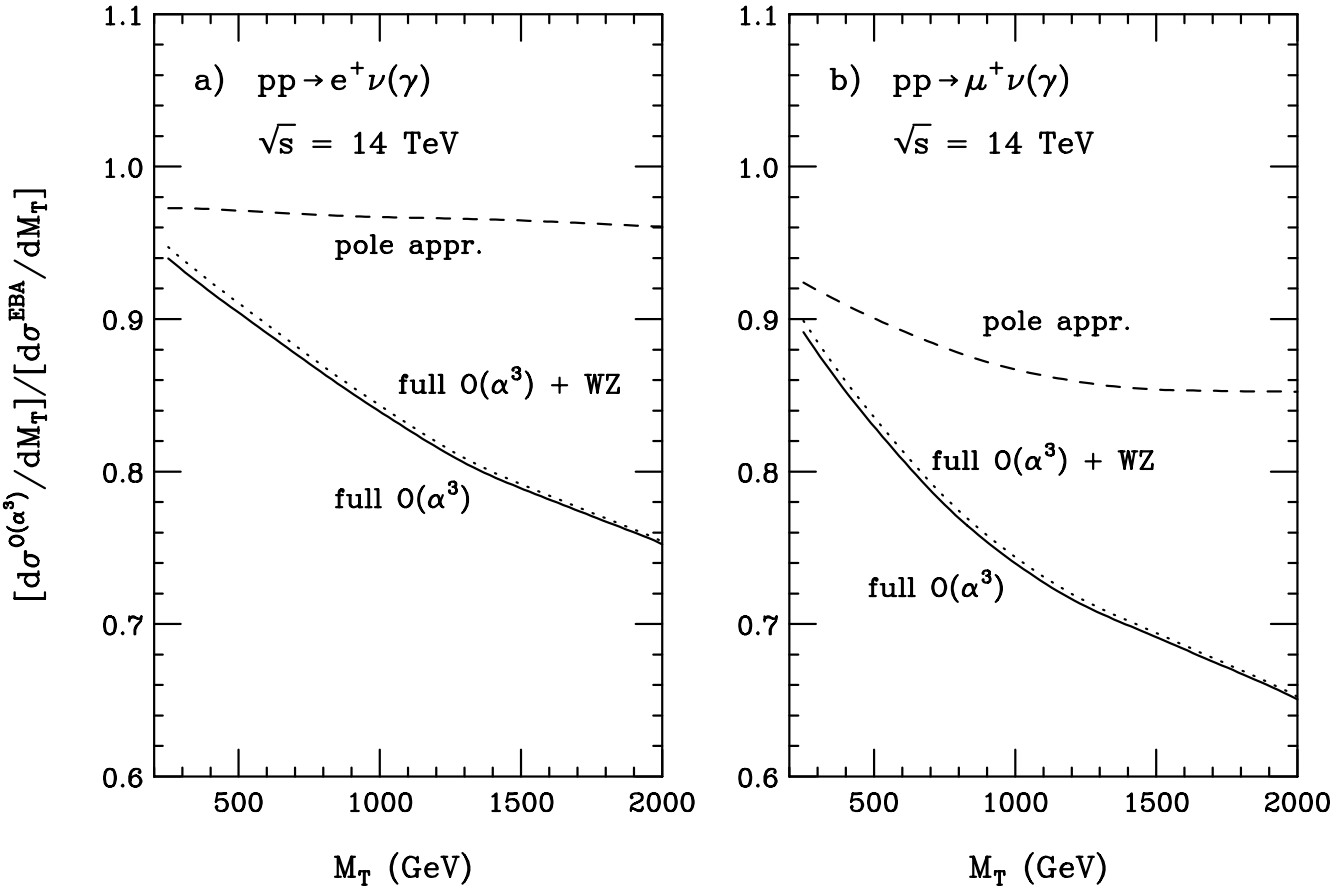

FIG. 5. The ratio $[d\sigma^{\mathcal{O}(\alpha^3)}/dM_T]/[d\sigma^{\mathrm{EBA}}/dM_T]$ as a function of the transverse mass for (a) $pp \to e^+\nu_e(\gamma)$ and (b) $pp \to \mu^+\nu_\mu(\gamma)$ at $\sqrt{s} = 14$ TeV. The solid lines show the ratio of the complete $\mathcal{O}(\alpha^3)$ electroweak and the EBA differential cross section. The dashed lines display the corresponding ratio for the case where only the resonant $\mathcal{O}(\alpha)$ EW corrections (see Eq. (4)) are taken into account (pole approximation). The dotted lines show the ratio when the $pp \to W^+(\to \ell^+\nu)Z(\to \bar{\nu}\nu)$ background is included in addition to the complete $\mathcal{O}(\alpha^3)$ EW corrections. The cuts and lepton identification requirements imposed are described in Sec. III A.

$\mathcal{R}(\Gamma_W)$. However, detector resolution effects largely dilute this effect. Above the W mass, $\mathcal{R}_{\mathrm{PA}}(\Gamma_W)$ rapidly drops from $\mathcal{R}_{\mathrm{PA}}(\Gamma_W) \approx 1$ to $\mathcal{R}_{\mathrm{PA}}(\Gamma_W) \approx \Gamma_W/\Gamma_W^{\mathrm{SM}}$. The M_T range over which the transition occurs sensitively depends on the missing transverse momentum resolution of the detector.

The solid line in Fig. 6 shows the ratio

$$\mathcal{R}_{\mathrm{PA}}^{\mathcal{O}(\alpha^3)} = (d\tilde{\sigma}^{\mathcal{O}(\alpha^3)}/dM_T)/(d\tilde{\sigma}^{\mathrm{PA}}/dM_T), \tag{23}$$

for $\Gamma_W = \Gamma_W^{\mathrm{SM}}$, where $d\tilde{\sigma}^{\mathcal{O}(\alpha^3)}/dM_T$ and $d\tilde{\sigma}^{\mathrm{PA}}/dM_T$ are the SM normalized M_T distributions for the complete $\mathcal{O}(\alpha^3)$ calculation and in the pole approximation, respectively. The data points and error bars in Fig. 6 indicate the measurements and statistical uncertainties expected for $\mathcal{R}_{\mathrm{PA}}^{\mathcal{O}(\alpha^3)}$ for 20 GeV bins and an integrated luminosity of 2 fb^{-1}, assuming that the data are described by the SM prediction including the full $\mathcal{O}(\alpha)$ EW corrections. Because of the nonresonant EW corrections, $\mathcal{R}_{\mathrm{PA}}^{\mathcal{O}(\alpha^3)}$ gradually decreases for $M_T > 90$ GeV, the region used by the Tevatron experiments to extract the W width from Run I data [16,17]. Although the shape change of the transverse mass distribution due to the nonresonant $\mathcal{O}(\alpha)$ EW correction differs significantly from that caused by a nonstandard W width, the expected statistical uncertainties make it difficult to distinguish between a small negative shift in Γ_W and the effect of nonresonant $\mathcal{O}(\alpha)$ EW corrections. A χ^2 analysis shows that, were the nonresonant $\mathcal{O}(\alpha)$ EW corrections ignored, the value of the W width extracted from the $M_T > 90$ GeV data region would be shifted by

$$\Delta\Gamma_W = -7.2 \text{ MeV}. \tag{24}$$

Since the M_T distribution depends little on the detector resolution for $M_T > 90$ GeV, the shift in Γ_W is almost independent of these effects [7]. For the precision of Γ_W expected in Run II, a difference of ≈ 7 MeV in the extracted value of the W width cannot be ignored, and the complete $\mathcal{O}(\alpha^3)$ calculation should be used to compare theory and data.

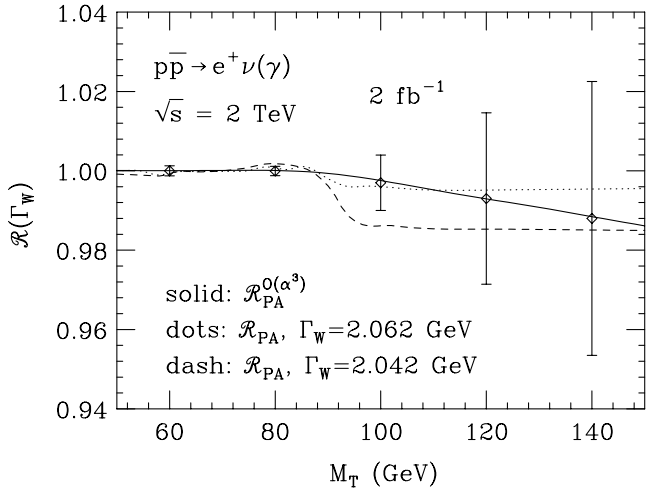

FIG. 6. The ratio $\mathcal{R}(\Gamma_W)$ (see text for definition) as a function of M_T for $p\bar{p} \to e^+\nu(\gamma)$ at the Tevatron. Results are shown for $\Gamma_W = \Gamma_W^{\rm SM} - 10$ MeV $= 2.062$ GeV (dotted line) and $\Gamma_W = \Gamma_W^{\rm SM} - 30$ MeV $= 2.042$ GeV (dashed line) with the cross sections calculated in the pole approximation. The solid line displays the ratio $\mathcal{R}_{\rm PA}^{\mathcal{O}(\alpha^3)} = [d\tilde{\sigma}^{\mathcal{O}(\alpha^3)}/dM_T]/[d\tilde{\sigma}^{PA}/dM_T]$ in the SM. The data points and error bars indicate the measurements and statistical uncertainties expected for $\mathcal{R}_{\rm PA}^{\mathcal{O}(\alpha^3)}$ for 20 GeV bins and an integrated luminosity of 2 fb^{-1}, assuming that the data are described by the SM prediction including the full $\mathcal{O}(\alpha)$ EW corrections. The cuts and lepton identification requirements imposed are described in Sec.III A.

E. Nonresonant Corrections to the W Boson Cross Section and the W to Z Cross Section Ratio

As mentioned in Sec. I, the W width can also be determined from the cross section ratio $R_{W/Z}$ (see Eq. (1)), together with the theoretical prediction for the ratio of the total W and Z production cross sections, the LEP measurement of the $Z \to \ell^+\ell^-$ branching ratio, and the SM prediction for the $W \to \ell\nu$ decay width. Since the QCD corrections to W and Z production are very similar, they cancel almost perfectly in the W to Z cross section ratio; the $\mathcal{O}(\alpha_s)$ corrections to $R_{W/Z}$ are of $\mathcal{O}(1\%)$ or less, depending on the set of parton distribution functions used [56]. In addition many experimental uncertainties, such as the luminosity uncertainty, cancel in the cross section ratio. Accurate knowledge of how electroweak corrections affect $R_{W/Z}$ is thus very important.

The W cross section may be used as a luminosity monitor in the future [57,58]. This requires that the W cross section is reliably computed with small uncertainty. In order to achieve this, it is essential to know how EW radiative corrections affect the $W \to \ell\nu$ cross section.

The size of the $\mathcal{O}(\alpha)$ electroweak corrections to the total $p\bar{p} \to \ell\nu X$ cross section and to $R_{W/Z}$ is sensitive to the acceptance cuts and whether lepton identification requirements are taken into account or not. In Table III, we list the electroweak K-factor,

$$K^{\rm EW} = \frac{\sigma^{\mathcal{O}(\alpha^3)}(p\bar{p} \to W \to \ell\nu X)}{\sigma^{\rm EBA}(p\bar{p} \to W \to \ell\nu)}, \tag{25}$$

and the correction factor for $R_{W/Z}$,

$$K_R^{\rm EW} = \frac{R_{W/Z}^{\mathcal{O}(\alpha^3)}}{R_{W/Z}^{\rm EBA}}, \tag{26}$$

for the acceptance cuts listed in Eqs. (14) and (15) with and without taking the lepton identification requirements of Table I into account. For $K^{\rm EW}$, we also list the result obtained in the pole approximation. To compute the $\mathcal{O}(\alpha^3)$ Z boson cross section entering $R_{W/Z}$, we use the full $\mathcal{O}(\alpha^3)$ calculation of di-lepton production in hadronic collisions described in Ref. [33]. We include photon exchange and γZ interference effects, and impose a cut on the di-lepton invariant mass of 75 GeV $< m(\ell^+\ell^-) <$ 105 GeV. The definition of the effective Born approximation in the Z case is given in Ref. [33]. The values listed in Table III update the results presented in Ref. [18] which were obtained using the pole approximation for the $W \to \ell\nu$ cross section and only included QED corrections in the Z boson case.

From the results listed in Table III one observes that the nonresonant $\mathcal{O}(\alpha)$ EW corrections have a very small effect on the W boson cross section; they change the electroweak K factor by $\mathcal{O}(10^{-3})$ or less. The full $\mathcal{O}(\alpha)$ EW corrections decrease the W cross section and increase

TABLE III. The electroweak K-factor $K^{\rm EW} = \sigma^{\mathcal{O}(\alpha^3)}(p\bar{p} \to W \to \ell\nu X)/\sigma^{\rm EBA}(p\bar{p} \to W \to \ell\nu)$ ($\ell = e, \mu$) and the correction factor to $R_{W/Z}$, $K_R^{\rm EW} = R_{W/Z}^{\mathcal{O}(\alpha^3)}/R_{W/Z}^{\rm EBA}$, with 75 GeV $< m(\ell^+\ell^-) <$ 105 GeV, for $p\bar{p}$ collisions at $\sqrt{s} = 2$ TeV. Shown are the predictions without and with the lepton identification requirements of Table I taken into account. The cuts imposed are listed in Eqs. (14) and (15). The energy and momentum resolutions used are described in Sec. III A.

	Without lepton id. requirements	With lepton id. requirements
$K^{\rm EW}(p\bar{p} \to e^+\nu X)$, full $\mathcal{O}(\alpha^3)$	0.963	0.984
$K^{\rm EW}(p\bar{p} \to e^+\nu X)$, pole appr.	0.963	0.984
$K^{\rm EW}(p\bar{p} \to \mu^+\nu X)$, full $\mathcal{O}(\alpha^3)$	0.979	0.944
$K^{\rm EW}(p\bar{p} \to \mu^+\nu X)$, pole appr.	0.978	0.943
$K_R^{\rm EW}(e)$, full $\mathcal{O}(\alpha^3)$	1.024	0.992
$K_R^{\rm EW}(\mu)$, full $\mathcal{O}(\alpha^3)$	1.002	1.045

$R_{W/Z}$ by several percent for the cuts imposed. When lepton identification requirements are included, the corrections are reduced in the electron case and enhanced in the muon case. Unlike the QCD corrections, the electroweak corrections do not cancel in $R_{W/Z}$. In $Z \to \ell^+\ell^-$ both leptons can emit photons, whereas only the charged lepton radiates in $W \to \ell\nu$ decays. Since final state photonic corrections are the dominating contribution to the $\mathcal{O}(\alpha)$ EW corrections, the $\mathcal{O}(\alpha)$ corrections to the W and Z cross sections are quite different, and therefore do not cancel in $R_{W/Z}$. They are of the same size as the QCD corrections to $R_{W/Z}$. The size of the $\mathcal{O}(\alpha)$ EW corrections to the total $p\bar{p} \to \ell\nu X$ cross section and to $R_{W/Z}$ is similar to the statistical uncertainty from 72 pb^{-1} of data from Run II [59]. It is thus important to take the EW radiative corrections into account in the Run II data analysis.

F. The Full $\mathcal{O}(\alpha)$ Electroweak Corrections to the W to Z Transverse Mass Ratio

Since detectors cannot directly detect the neutrinos produced in the leptonic W boson decays, $W \to \ell\nu$, and cannot measure the longitudinal component of the recoil momentum, there is insufficient information to reconstruct the invariant mass of the W boson. Instead, the transverse mass distribution of the final state lepton pair, or the transverse momentum distribution of the charged lepton are used [12,13] to extract M_W. The M_T distribution has the advantage of being invariant under transverse boosts to first order in the velocity of the W boson. On the other hand, the transverse mass depends on an accurate reconstruction of the neutrino direction which leads to a set of experimental requirements which are difficult in practice to control [7].

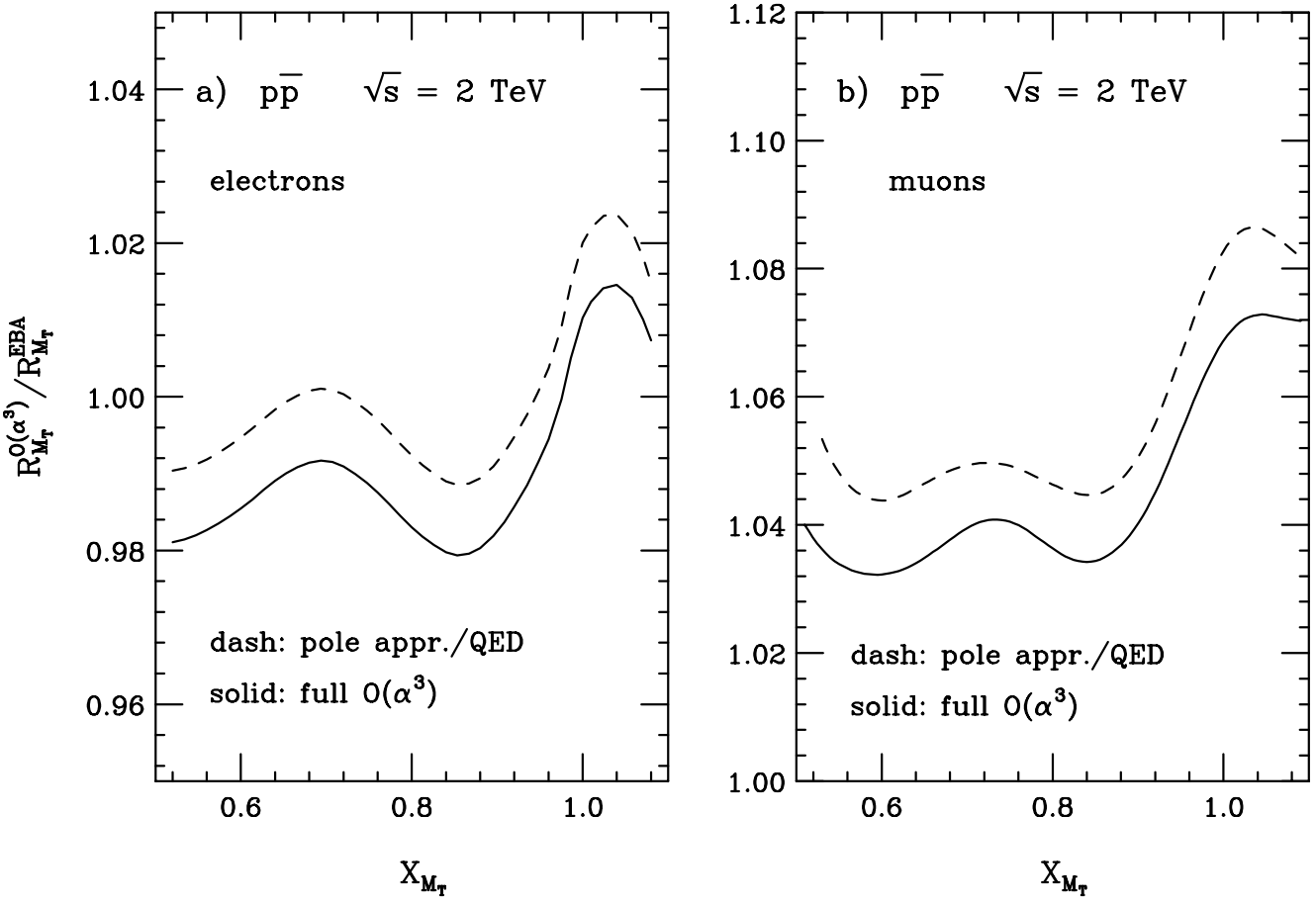

FIG. 7. Ratio of the $\mathcal{O}(\alpha^3)$ and the W^+ to Z transverse mass ratio in the effective Born approximation as a function of the scaled transverse mass, X_{M_T}, for $p\bar{p}$ collisions at $\sqrt{s} = 2$ TeV, (a) for electron, and (b) for muon final states. The solid lines show the result when the complete $\mathcal{O}(\alpha)$ EW radiative corrections are taken into account. The dashed lines give the result for the EW radiative corrections to W production in the pole approximation, and when only the QED corrections to Z boson production are taken into account (as in Ref. [18]). The cuts and lepton identification requirements imposed are described in Sec. III A. For $p\bar{p} \to \ell^+\ell^-(\gamma)$, we in addition require the di-lepton invariant mass to satisfy the constraint 75 GeV $< m(\ell^+\ell^-) <$ 105 GeV.

The W mass can also be determined from the ratio of the transverse mass distributions of the W and Z boson [60–62]. The advantage of this method is that one can cancel common scale factors in ratios and directly determine M_W/M_Z, which can be compared with the precise value of M_Z from the LEP experiments. The downside of the ratio method is that the statistical precision of the Z sample is directly propagated into the resultant overall uncertainty of M_W. At high luminosities, or when a detailed understanding of the detector response is not available, the transverse mass ratio of W to Z bosons offers advantages in determining the W mass over the M_T distribution [7].

The transverse mass ratio of W and Z bosons is defined as

$$R_{M_T}(X_{M_T}) = \frac{A_W(X^W_{M_T} = X_{M_T})}{A_Z(X^Z_{M_T} = X_{M_T})}, \tag{27}$$

where A_V ($V = W, Z$) is the differential cross section

$$A_V(X^V_{M_T}) = \frac{d\sigma_V}{dX^V_{M_T}} \tag{28}$$

with respect to the scaled transverse mass

$$X^V_{M_T} = \frac{M^V_T}{M_V}. \tag{29}$$

The transverse mass of the lepton pair in Z boson events is defined in complete analogy to Eq. (19):

$$M^Z_T = \sqrt{2p_T(\ell^+)p_T(\ell^-)(1 - \cos\phi^{\ell\ell})}, \tag{30}$$

where $\phi^{\ell\ell}$ is the angle between the two charged leptons in the transverse plane. The $\mathcal{O}(\alpha)$ EW radiative corrections to R_{M_T} were calculated in Ref. [18] in the approximation where only the QED corrections were taken into account for $Z \to \ell^+\ell^-$ and the pole approximation was used for $W \to \ell\nu$. Here we present results which include the complete $\mathcal{O}(\alpha)$ EW radiative corrections.

The ratio of the $\mathcal{O}(\alpha^3)$ and the W to Z transverse mass ratio in the effective Born approximation is shown in Fig. 7. To calculate the $\mathcal{O}(\alpha)$ electroweak corrections to Z boson production, we again use the results of Ref. [33]. As before, photon exchange and γZ interference effects are included and an additional cut on the di-lepton invariant mass of 75 GeV $< m(\ell^+\ell^-) <$ 105 GeV has been imposed. The complete $\mathcal{O}(\alpha)$ EW radiative corrections (solid lines) are uniformly about 1% smaller than those obtained when the pole approximation is used for W production and only QED corrections to Z boson production are taken into account (dashed lines). Most of this effect originates from the genuine weak corrections to the Z boson cross section. In the electron case, the $\mathcal{O}(\alpha)$ EW corrections change R_{M_T} by 1%–2%. They are larger in the muon case (3%–7%) due to the lepton identification requirements which reduce the hard photon part of the $\mathcal{O}(\alpha^3)$ cross section and thus enhance the effect of the virtual corrections. In the resonance region, $X_{M_T} \approx 1$, hard photonic corrections reduce both the W and Z boson cross sections. As mentioned before, in $p\bar{p} \to \ell\nu(\gamma)$ only one of the two leptons can emit a photon, whereas both leptons in $p\bar{p} \to \ell^+\ell^-(\gamma)$ can radiate. As a result, the effect of the hard photonic corrections is more pronounced in the Z case, resulting in a resonancelike enhancement of R_{M_T} for $X_{M_T} \approx 1$.

IV. CONCLUSIONS

We have presented a calculation of the $\mathcal{O}(\alpha)$ corrections to $p\overset{(-)}{p} \to W^\pm \to \ell^\pm\nu$ based on the complete set of one-loop Feynman diagrams contributing to $\ell\nu$ production, using the methods developed in Ref. [24]. The calculation is based on a combination of analytic and Monte Carlo integration techniques. Lepton mass effects are included in the approximation where only mass singular terms originating from the collinear singularity associated with final state photon radiation are retained. The ultraviolet divergences associated with the virtual corrections are regularized using dimensional regularization and the ON SHELL renormalization scheme [31]. The cross sections obtained using our matrix elements were found to be in very good agreement with those obtained in Ref. [19].

Since the structure of the full $\mathcal{O}(\alpha^3)$ matrix elements and the $\mathcal{O}(\alpha)$ EW corrections in the pole approximation were discussed in detail in earlier papers [18,19], we concentrated on the phenomenological effects of the nonresonant corrections. The nonresonant corrections were found to have a very small effect on the total W cross section and the transverse mass distribution in the region $M_T \leq M_W$. However, they increase rapidly in magnitude with M_T above the W peak, due to the presence of Sudakov-like electroweak logarithms. Although these corrections are of moderate size for transverse masses accessible at the Tevatron, they induce a shift of $\Delta\Gamma_W \approx -7$ MeV in the W width extracted from the tail of the transverse mass distribution. Comparison with the expected overall precision of about $\delta\Gamma_W = 25$–30 MeV in Run II of the Tevatron shows that it will be necessary to take the nonresonant electroweak corrections into account in the data analysis. For transverse masses in the TeV region which play an important role in new physics searches at the LHC, the nonresonant electroweak corrections are of the same size as the $\mathcal{O}(\alpha_s)$ corrections. The strong increase of these corrections with M_T requires that they are resummed. No such calculation exists yet for $\ell\nu$ production in hadronic collisions.

We also updated the results of the electroweak K-factor for the W/Z cross section ratio $R_{W/Z}$ and the W to Z transverse mass ratio given in Ref. [18] to include the complete $\mathcal{O}(\alpha)$ EW radiative corrections and the

$\mathcal{O}(g^4 m_t^2/M_W^2)$ corrections to the Z boson cross section [33].

ACKNOWLEDGMENTS

We would like to thank S. Dittmaier, Y. K. Kim, A. Kotwal, K. McFarland, M. Krämer, and W. Trischuk for useful discussions. We also would like to thank the Kavli Institute for Theoretical Physics and the Fermilab Theory Group, where part of this work was done, for their generous hospitality and for financial support. This research was supported in part by the U.S. Department of Energy under Contract No. DE-AC02-76CH03000, and the National Science Foundation under Grant No. PHY-99-07949, No. PHY-0139953, and No. PHY-0244875.

APPENDIX A: THE PURELY WEAK CONTRIBUTION

The pure weak vertex and self-energy one-loop corrections to the process described by the form factor $F_{\rm weak}$ of Eq. (2) can be decomposed into initial and final state contributions as follows:

$$F_{\rm weak}(\hat{s}) = F_{\rm weak}^{\rm initial}(\hat{s}) + F_{\rm weak}^{\rm final}(\hat{s}) \tag{A1}$$

with the final state contribution

$$F_{\rm weak}^{\rm final}(\hat{s}) = \sum_{j=I,II,III} F_{j,f}^{\rm weak}(\hat{s}) + \delta Z_1^W - \delta Z_2^W - \frac{1}{2}\frac{\Sigma_T^{W,\rm weak}(\hat{s}) - \Sigma_T^{W,\rm weak}(M_W^2)}{\hat{s} - M_W^2} - \frac{1}{2}\delta Z_2^{W,\rm weak}. \tag{A2}$$

Performing the substitution $(f, f') \to (i, i')$ yields the corresponding initial state form factor $F_{\rm weak}^{\rm initial}(\hat{s})$. The explicit expressions for the various terms in Eq. (A2) can be found in Ref. [24].

The pure weak box contribution consisting of the WZ box diagrams of Fig. 2 in the limit of massless external fermions reads

$$d\hat{\sigma}_{WZ\rm box}(\hat{s}, \hat{t}) = \frac{\alpha}{\pi} d\hat{\sigma}^{(0)}(\hat{s}, \hat{t})(\hat{s} - M_W^2) \times \sum_{V1,V2=Z,W} \mathcal{R}e(\delta B_{V1V2} + \delta B_{V1V2}^{\rm crossed}) \tag{A3}$$

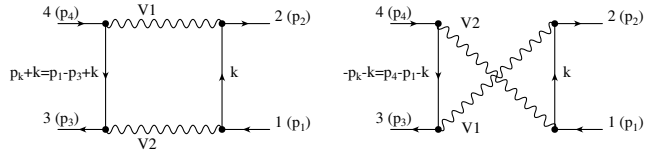

FIG. 8. Notations used in the calculation of the $V1, V2$ box diagrams.

with

$$\begin{aligned}\delta B_{V1V2}(\hat{s}, \hat{t}) &= \lambda_{V1V2}[2D_2^0 + \hat{t}(D_1^1 + D_1^2 + D_1^3 + D_2^2 + D_2^{23} + D_2^{12})],\\ \delta B_{V1V2}^{\rm crossed}(\hat{s}, \hat{u}) &= \lambda_{V1V2}^c[8D_2^0 + \hat{u}(D_1^1 + 2D_1^2 + D_1^3 + 2(D_2^2 + D_2^{23} + D_2^{12})) - 2\hat{s}D_2^{13})],\end{aligned} \tag{A4}$$

where $D_i^{j(k)} = D_i^{j(k)}(\hat{s}, \hat{t}, 0, M_{V1}, 0, M_{V2})$ in case of the box δB_{V1V2} and $D_i^{j(k)} = D_i^{j(k)}(\hat{s}, \hat{u}, 0, M_{V1}, 0, M_{V2})$ in case of the crossed box contribution $\delta B_{V1V2}^{\rm crossed}$. λ_{V1V2} and λ_{V1V2}^c contain the dependence on the vector and axial vector parts of the fermion-Z boson couplings which, in the notation of Fig. 8, are given by

$$\begin{aligned}\lambda_{WZ} &= 2(v_1 + a_1)(v_3 + a_3),\\ \lambda_{ZW} &= 2(v_2 + a_2)(v_4 + a_4),\\ \lambda_{WZ}^c &= 2(v_1 + a_1)(v_4 + a_4),\\ \lambda_{ZW}^c &= 2(v_2 + a_2)(v_3 + a_3),\end{aligned} \tag{A5}$$

with $v_i = (I_3^i - 2s_w^2 Q_i)/(2s_w c_w)$ and $a_i = I_3^i/(2s_w c_w)$ parametrizing the $Zf\bar{f}$ $(f = \ell, q)$ couplings. Here, Q_i and I_3^i denote the charge and third component of the weak isospin quantum numbers of the fermion i, and $s_w = \sin\theta_W$, $c_w = \cos\theta_W$ with θ_W being the weak mixing angle.

The box integrals arising in the calculation of the Feynman diagrams of Fig. 8 are of the form

$$\frac{i}{16\pi^2}(D_0, D^\mu, D^{\mu\nu}) = \int \frac{d^4k}{(2\pi)^4} \frac{(1, k^\mu, k^\mu k^\nu)}{[k^2 + i\epsilon][(k - p_2)^2 - M_{V1}^2][(k + p_k)^2 + i\epsilon][(k + p_1)^2 - M_{V2}^2]}. \tag{A6}$$

The explicit decomposition of the vectorial and tensorial four point functions

$$D^{\mu} = -p_2^{\mu} D_1^1 + p_k^{\mu} D_1^2 + p_1^{\mu} D_1^3,$$
$$D^{\mu\nu} = p_2^{\mu} p_2^{\nu} D_2^1 + p_k^{\mu} p_k^{\nu} D_2^2 + p_1^{\mu} p_1^{\nu} D_2^3 + g^{\mu\nu} D_2^0 - (p_2^{\mu} p_k^{\nu} + p_k^{\mu} p_2^{\nu}) D_2^{12} - (p_2^{\mu} p_1^{\nu} + p_1^{\mu} p_2^{\nu}) D_2^{13} + (p_k^{\mu} p_1^{\nu} + p_1^{\mu} p_k^{\nu}) D_2^{23} \tag{A7}$$

can be found in Ref. [63].

[1] LEPEWWG Collaboration, D. Abbaneo *et al.*, hep-ex/0312023; http://lepewwg.web.cern.ch/LEPEWWG.
[2] The LEP Collaborations, R. Barate *et al.*, Phys. Lett. B **565**, 61 (2003).
[3] L. Demortier *et al.*, Fermilab Report No. FERMILAB-TM-2084, 1999 (unpublished); TEVEWWG Collaboration, P. Azzi *et al.*, hep-ex/0404010.
[4] S. Eidelman and F. Jegerlehner, Z. Phys. C **67**, 585 (1995); K. Hagiwara, A. D. Martin, D. Nomura, and T. Teubner, Phys. Rev. D **69**, 093003 (2004), and references therein.
[5] R. Clare, in LoopFest III, KITP, Santa Barbara, 2004 (unpublished); S. Roth, in *Proceedings of the XXXIXth Rencontres de Moriond: QCD and Hadronic Interactions at High Energy, La Thuile, Italy, 2004* (unpublished).
[6] U. Baur *et al.*, in *Proceedings of the APS/DPF/DPB Summer Study on the Future of Particle Physics (Snowmass, 2001)*, edited by N. Graf., eConf C010630, P122 (2001), and references therein.
[7] R. Brock *et al.*, hep-ex/0011009.
[8] D0 Collaboration, S. Abachi *et al.*, Phys. Rev. Lett. **75**, 1456 (1995).
[9] CDF Collaboration, F. Abe *et al.*, Phys. Rev. Lett. **73**, 220 (1994); Phys. Rev. D **52**, 2624 (1995).
[10] C. Balazs and C. P. Yuan, Phys. Rev. D **56**, 5558 (1997); R. K. Ellis and S. Veseli, Nucl. Phys. **B511**, 649 (1998), and references therein.
[11] F. Landry, R. Brock, G. Ladinsky, and C. P. Yuan, Phys. Rev. D **63**, 013004 (2001).
[12] CDF Collaboration, F. Abe *et al.*, Phys. Rev. Lett. **75**, 11 (1995); Phys. Rev. D **52**, 4784 (1995); CDF Collaboration, T. Affolder *et al.*, Phys. Rev. D **64**, 052001 (2001).
[13] D0 Collaboration, S. Abachi *et al.*, Phys. Rev. Lett. **77**, 3309 (1996); D0 Collaboration, B. Abbott *et al.*, Phys. Rev. D **58**, 012002 (1998); Phys. Rev. D **58**, 092003 (1998); Phys. Rev. Lett. **80**, 3008 (1998); Phys. Rev. Lett. **84**, 222 (2000); Phys. Rev. D **62**, 092006 (2000); D0 Collaboration, V. M. Abazov *et al.*, Phys. Rev. D **66**, 012001 (2002).
[14] TEVEWWG Collaboration, W. Ashmanskas *et al.*, hep-ex/0311039, and references therein.
[15] CDF Collaboration, F. Abe *et al.*, Phys. Rev. Lett. **74**, 341 (1995).
[16] CDF Collaboration, T. Affolder *et al.*, Phys. Rev. Lett. **85**, 3347 (2000).
[17] D0 CollaborationV. M. Abazov *et al.*, Phys. Rev. D **66**, 032008 (2002).
[18] U. Baur, S. Keller, and D. Wackeroth, Phys. Rev. D **59**, 013002 (1999).
[19] S. Dittmaier and M. Krämer, Phys. Rev. D **65**, 073007 (2002).
[20] U. Baur and T. Stelzer, Phys. Rev. D **61**, 073007 (2000).
[21] C. M. Carloni Calame, G. Montagna, O. Nicrosini, and M. Treccani, Phys. Rev. D **69**, 037301 (2004).
[22] W. Placzek and S. Jadach, Eur. Phys. J. C **29**, 325 (2003).
[23] Q. H. Cao and C. P. Yuan, Phys. Rev. Lett. **93**, 042001 (2004).
[24] D. Wackeroth and W. Hollik, Phys. Rev. D **55**, 6788 (1997).
[25] U. Baur and D. Wackeroth, Nucl. Phys. B, Proc. Suppl. **116**, 159 (2003).
[26] H. Baer, J. Ohnemus, and J. F. Owens, Phys. Rev. D **40**, 2844 (1989); Phys. Rev. D **42**, 61 (1990); B. W. Harris and J. F. Owens, Phys. Rev. D **65**, 094032 (2002).
[27] A. de Rújula, R. Petronzio, and A. Savoy-Navarro, Nucl. Phys. **B154**, 394 (1979).
[28] J. Kripfganz and H. Perlt, Z. Phys. C **41**, 319 (1988).
[29] H. Spiesberger, Phys. Rev. D **52**, 4936 (1995).
[30] M. Roth and S. Weinzierl, Phys. Lett. B **590**, 190 (2004).
[31] M. Böhm, W. Hollik, and H. Spiesberger, Fortschr. Phys. **34**, 687 (1986).
[32] P. Ciafaloni and D. Comelli, Phys. Lett. B **446**, 278 (1999).
[33] U. Baur, O. Brein, W. Hollik, C. Schappacher, and D. Wackeroth, Phys. Rev. D **65**, 033007 (2002).
[34] T. Kinoshita, J. Math. Phys. (N.Y.) **3**, 650 (1962); T. D. Lee and M. Nauenberg, Phys. Rev. **133**, 1549 (1964).
[35] V. N. Gribov and L. N. Lipatov, Sov. J. Nucl. Phys. **15**, 438 (1972); **15**, 675 (1972); G. Altarelli and G. Parisi, Nucl. Phys. **B126**, 298 (1977).
[36] S. Haywood, P. Hobson, W. Hollik, Z. Kunszt *et al.*, "Electroweak Physics," in Proceedings of the Workshop on Standard Model Physics (and more) at the LHC, CERN, Geneva, Switzerland, 1999, edited by G. Altarelli and M. Mangano (unpublished), hep-ph/0003275.
[37] A. D. Martin, R. G. Roberts, W. J. Stirling, and R. S. Thorne, Eur. Phys. J. C **23**, 73 (2002).
[38] J. Pumplin, D. R. Stump, J. Huston, H. L. Lai, P. Nadolsky, and W. K. Tung, J. High Energy Phys. 07 (2002) 012.
[39] W. A. Bardeen, A. J. Buras, D. W. Duke, and T. Muta, Phys. Rev. D **18**, 3998 (1978).
[40] J. F. Owens and W. K. Tung, Annu. Rev. Nucl. Part. Sci. **42**, 291 (1992).

[41] Particle Data Group, C. Caso *et al.*, Eur. Phys. J. C **3**, 1 (1998).
[42] M. Awramik, M. Czakon, A. Freitas, and G. Weiglein, Phys. Rev. D **69**, 053006 (2004).
[43] G. Degrassi, P. Gambino, M. Passera, and A. Sirlin, Phys. Lett. B **418**, 209 (1998).
[44] A. Ferroglia, G. Ossola, M. Passera, and A. Sirlin, Phys. Rev. D **65**, 113002 (2002).
[45] A. Denner and T. Sack, Z. Phys. C **46**, 653 (1990), and references therein.
[46] K. G. Chetyrkin, A. L. Kataev, and F.V. Tkachov, Phys. Lett. **85B**, 277 (1979); M. Dine and J. Sapirstein, Phys. Rev. Lett. **43**, 668 (1979); W. Celmaster and R. J. Gonsalves, Phys. Rev. Lett. **44**, 560 (1980); S. G. Gorishnii, A. L. Kataev, and S. A. Larin, Phys. Lett. B **259**, 144 (1991); L. R. Surguladze and M. A. Samuel, Phys. Rev. Lett. **66**, 560 (1991); K. G. Chetyrkin, J. H. Kühn, and A. Kwiatkowski, hep-ph/9503396.
[47] A. L. Kataev, Phys. Lett. B **287**, 209 (1992).
[48] A. D. Martin, R. G. Roberts, and W. J. Stirling, Phys. Lett. B **387**, 419 (1996).
[49] CDF Collaboration, F. Abe *et al.*, Fermilab Report No. FERMILAB-Pub-96/390-E, 1996 (unpublished).
[50] D0 Collaboration, S. Abachi *et al.*, Fermilab Report No. FERMILAB-Pub-96/357-E, 1996 (unpublished).
[51] ATLAS Collaboration, A. Airapetian *et al.*, CERN Report No. CERN/LHCC/99-14, 1999 (unpublished).
[52] CMS Collaboration, M. Della Negra *et al.*, CMS Letter of Intent, CERN Report No. CERN-LHCC-92-3, 1992 (unpublished); CMS Collaboration, G. L. Bayatian *et al.*, CMS Technical Design, CERN Report No. CERN-LHCC-94-38, 1994 (unpublished).
[53] G. Polesello and M. Prata, Report No. SN-ATLAS-2003-036.
[54] M. Melles, Phys. Rep. **375**, 219 (2003), and references therein.
[55] J. H. Kühn, S. Moch, A. A. Penin, and V. A. Smirnov, Nucl. Phys. **B616**, 286 (2001); **B648**, 455(E) (2003); J. H. Kühn, A. A. Penin, and V. A. Smirnov, Eur. Phys. J. C **17**, 97 (2000); M. Beccaria, P. Ciafaloni, D. Comelli, F. M. Renard, and C. Verzegnassi, Phys. Rev. D **61**, 073005 (2000); J. H. Kühn and A. A. Penin, hep-ph/9906545.
[56] W. L. van Neerven and E. B. Zijlstra, Nucl. Phys. **B382**, 11 (1992).
[57] CDF Collaboration, F. Abe *et al.*, Phys. Rev. Lett. **76**, 3070 (1996).
[58] M. Dittmar, F. Pauss, and D. Zürcher, Phys. Rev. D **56**, 7284 (1997).
[59] TEVEWWG Collaboration, S. Eno *et al.*, Report No. CDF6566, D0 Note 4188, 2003 (unpublished).
[60] S. Rajagopalan and M. Rijssenbeek, "*Measurement of the W Mass Using the Transverse Mass Ratio of the W and Z*," D0 Note 3000, 1996 (unpublished); S. Rajagopalan, "Measurement of the *W* Mass Using the Transverse Mass Ratio of the *W* and *Z*," Division of Particles and Fields Conference, 1996.
[61] W. T. Giele and S. Keller, Phys. Rev. D **57**, 4433 (1998).
[62] D. Shpakov, Ph.D. thesis, Stony Brook, 2000.
[63] A. Denner and T. Sack, Nucl. Phys. **B306**, 221 (1988).
[64] W. F. L. Hollik, Fortschr. Phys. **38**, 165 (1990).